Petroleum Science 22 (2025) 3005–3014

Contents lists available at ScienceDirect

Petroleum Science

journal homepage: www.keaipublishing.com/en/journals/petroleum-science

Original Paper

Research on the semi-empirical model for predicting the geometrical deformation of the sealing discs of pipeline inspection gauge

Xiao-Xiao Zhu [a,b,*], Hao-Kun Wang [c], Yi-Chen Zhang [c], Chun-Ming Fu [c], Li-Yun Lao [d]

[a] College of Safety and Ocean Engineering, China University of Petroleum (Beijing), Beijing, 102249, China
[b] Key Laboratory of Oil and Gas Safety and Emergency Technology, Ministry of Emergency Management, Beijing, 102249, China
[c] College of Mechanical and Transportation Engineering, China University of Petroleum (Beijing), Beijing, 102249, China
[d] Centre for Thermal Energy Systems and Materials, Cranfield University, Cranfield, Bedfordshire, MK43 0AL, UK

A R T I C L E I N F O

Article history:
Received 22 July 2024
Received in revised form
5 December 2024
Accepted 19 May 2025
Available online 21 May 2025

Edited by Teng Zhu

Keywords:
Pipeline pigging
Frictional force
Sealing disc
Deformation
Mathematical model

A B S T R A C T

Pipeline Inspection Gauge (pig) is an important equipment for oil and gas pipelines during different stages of their operations to perform functions such as dewatering, cleaning, and inspection. Owing to the hyperelasticity, time and temperature-dependent material behaviour of the sealing disc attached on the pig, the contact between the pig and the pipeline expresses complex behaviour, leading to an uncertainty in the prediction of the pig's frictional force. Knowing the deformation of the sealing discs well is essential and can be highly meaningful for predicting the pig motion, as well as reducing the pigging risks. In this study, the geometrical deformation of the sealing discs with different sizes are investigated through experiments and numerical simulations. The effects of the four nondimensionalized parameters (interference, thickness per pipeline inner diameter, and clamping ratio) of the sealing discs on the deformation behaviour were observed and discussed, and an improved mathematical model for predicting the geometrical deformation of the sealing discs was proposed and verified. With the auxiliary angle α added in the improved mathematical model, the relative error declines to 1.87% and 3.18% respectively for predicting deformation of the sealing discs in size of 2-inch and 40-inch pig. The results of this study can help better understand the frictional force of a pig with sealing discs, as well as its motion.

1. Introduction

Onshore and offshore pipelines are the safest methods to transport oil and gas products (Saeidbakhsh et al., 2009; Lesani et al., 2012). However, the long usage time of these aging pipelines has raised serious concerns regarding their safety. Debris such as wax deposition or hydrate formation build-up in the pipeline reduces transportation efficiency; defects such as surface pitting or solid particle-induced erosion can damage the pipeline and cause various potential risks (Liu et al., 2019; Ciszewski et al., 2020). As a result, the standard procedure is to remove the debris in the pipeline regularly and check for corrosion, internal damage, wall thickness, pipe roundness, and cracks to enhance their safety and integrity in service (Botros and Golshan, 2009; Solghar and Davoudian, 2013; Wang et al., 2018).

Pipeline inspection gauges (pigs) are commonly used in oil and gas pipelines for cleaning and inspection during different stages of operation. They can be classified into normal pigs and intelligent pigs, depending on their functions (Tiratsoo, 1992, 2013; Rahe, 2006; Sadovnychiy et al., 2006), as shown in Fig. 1.

Pigs are often driven by the fluid in the pipeline, as shown in Fig. 2. Soft sealing discs or cups (often made of polyurethane) attached to the pig interfere with the pipeline. Consequently, they can deform and seal the pipeline to build different pressures; thus, frictional resistance can be overcome, and the pig can be propelled to run in the pipeline with speed (Zhu et al., 2016, 2017a, 2017b, 2023a).

Owing to the hyperelasticity, time and temperature-dependent material behaviour of the sealing disc, unknown pipeline internal conditions, the sliding velocity, and presence of lubricants, the contact between the sealing disc and pipeline exhibits complex

* Corresponding author. College of Safety and Ocean Engineering, China University of Petroleum (Beijing), Beijing, 102249, China.
E-mail address: x.zhu@cup.edu.cn (X.-X. Zhu).

https://doi.org/10.1016/j.petsci.2025.05.013

Fig. 1. Normal pigs and intelligent pigs used for the pigging operation.

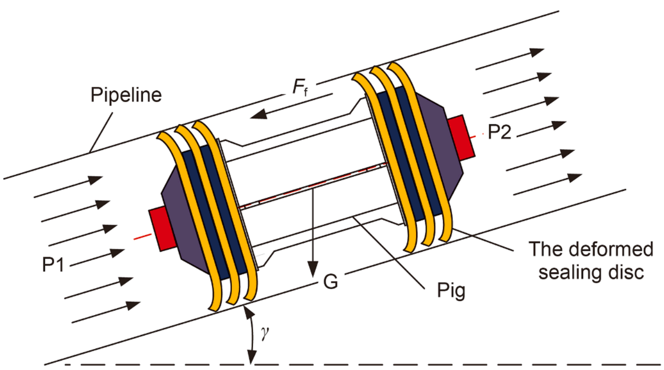

Fig. 2. Bi-directional pig when running through the pipeline (Zhu et al., 2015b).

behavior, leading to an uncertain prediction on the pigging motion in the pipeline (Niechele et al., 2000; Zhao et al., 2016; Zhang et al., 2022; Chang et al., 2023). Pigging risks cannot be defined in advance because the motion of pigs, such as pig velocity, position, and required driving pressure, especially in risers with severe slugging inside, are unclear (Li et al., 2021, 2024; Liu et al., 2022; Zhu et al., 2023b).

The resistance force of a pig running through a pipeline plays an important role in determining its motion, as shown in Eq. (1).

$$m\frac{\mathrm{d}V_{\mathrm{pig}}}{\mathrm{d}t} = \Delta P{\cdot}A - F_{\mathrm{f}} - m{\cdot}g{\cdot}\sin\gamma \tag{1}$$

Here, V_{pig} is the speed of the pig, m is its mass, ΔP is the differential pressure over the pig, A is the cross-sectional area of the pig that the differential pressure acting on, γ is the angle between the axis of the pig and the horizontal line, which is the angle between the horizontal direction and the counterclockwise direction of the pig (shown in Fig. 1), and F_{f} is the total resistance force between the sealing discs and the pipe inner surface.

The total resistance force of a pig (F_{f}) consists of the wax removal force (f_{w}), viscous force of the fluid (f_{v}), and the frictional force (f_{μ}) resulting from the soft contact between the rubber and the rigid pipe wall (Zhu et al., 2015a, 2017a). Wax removal force has been widely investigated in recent years (Souza Mendes et al., 1999; Wang et al., 2005; Banki et al., 2008; Wang et al., 2008; Bai and Zhang, 2013; Wang and Huang, 2014; Wang et al., 2014; Tan et al., 2014; Lan et al., 2016; Yu et al., 2020; Gao et al., 2021). However, research on the frictional force between pigs and pipelines is limited.

In previous studies, the frictional force in the pigging models proposed by Nguyen (Nguyen et al., 2001a, 2001b, 2001c), Tolmasquim (Tolmasquim and Nieckele, 2008) and Nieckele (Nieckele et al., 2001) were classified into static and dynamic forces without providing detailed calculations. Esmaeilzadeh (Esmaeilzadeh et al., 2006) obtained the frictional force of a foam pig using a shrink fit correlation. Romagnoli and Varvelli (1991), (Dai and Tao (2008), Liu (2010), de Souza et al. (2013) and Cao et al. (2018)) investigated the deformation of a cup pig (bowl-shaped rubber), and the contact force was estimated. Subsequently, the driving force of the bidirectional pig was investigated based on the four-element model, and the effect of the pigging velocity on it was observed (Liu et al., 2021). Zhu et al. (Zhu et al., 2015a, 2015b) proposed a nonlinear numerical model verified experimentally to estimate the frictional force of a bidirectional pig. The contact force and frictional coefficient were then experimentally investigated to reveal the contact behaviours of a bidirectional pig with sealing discs of different sizes (Zhu et al., 2017a). Ohwoka (2015) and Den Heijer (2016) conducted pull tests using different methods to evaluate the frictional force of a bidirectional pig. Hendrix (2018) presented a static experimental setup for measuring the frictional force and normal force acting on the sealing disc. In the above studies, the frictional force of a pig in a pipe was estimated using finite element simulation and/or experiments.

A mathematical model could be much more desirable in terms of time and cost effectiveness. O'Donoghue, (1996) proposed a simplified mathematical model which included the geometrical and material properties of the sealing disc into a friction model. In O′ Donoghue's model, the deformation of the sealing disc was assumed to be an ideal arc. Its centre angle was consequently larger, and the radius was smaller, compared with the parameters of the real arc (the details are shown in Section 2.1). In this study, the geometrical deformation of the sealing discs (the same kind of sealing discs that used in O'Donoghue's research) with various sizes were investigated. An improved model based on that proposed by O'Donoghue et al. was established and verified. The proposed model can predict the frictional force of a bidirectional pig with improved accuracy.

2. Mathematical model

2.1. O'Donoghue's model

O'Donoghue's mathematical model for describing the geometrical deformation of a sealing disk is based on the assumption that the deformed sealing disc adopts the shape of a circular arc (O'Donoghue, 1996; Hendrix et al., 2018), as shown in Fig. 3.

The geometrical equations for describing the deformed sealing disc can be expressed according to Eq. (2) and Eq. (3) as follows:

$$l = \frac{D_{\mathrm{S}} - D_{\mathrm{P}}}{2} \tag{2}$$

$$l' = \frac{d - D_{\mathrm{P}}}{2} - \frac{t}{2}\sin\beta \tag{3}$$

where D_{s} is the outer diameter of the sealing disc, D_{p} is the outer diameter of the separating disc, t is the thickness of the sealing disc, D is the inner diameter of the pipeline, and β is the centre

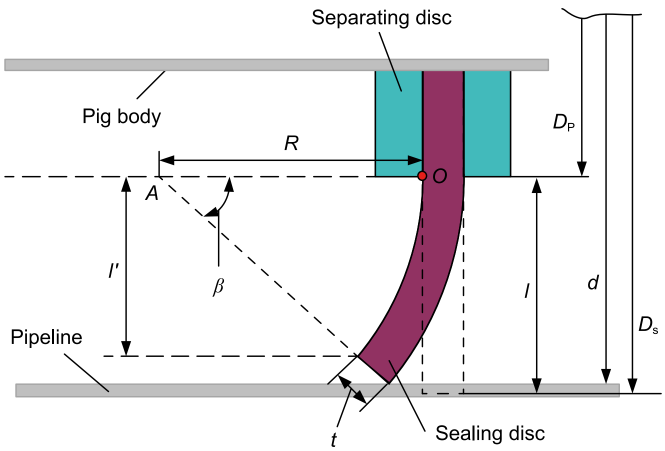

Fig. 3. Geometrical deformation model of the sealing disc proposed by O'Donoghue.

angle of the arc formed by the deformed sealing disc. The original and deflected lengths of the deformed sealing disc are l and l'.

Here, Eqs. (4)–(6) can be obtained from Fig. 3.

$$R \cdot \beta = l \tag{4}$$

$$R \cdot \sin\beta = l' \tag{5}$$

$$R = \frac{l}{\beta} = \frac{l'}{\sin\beta} = \frac{D_S - D_P}{2\beta} = \frac{d - D_P - t\sin\beta}{2\sin\beta} \tag{6}$$

where R is the radius of the arc formed by the deformed sealing disc.

However, the experimental and simulation results show that the deflected length is not an ideal arc, as shown in Figs. 4 and 5 (the experimental and simulation details are presented in Section 3). In O'Donoghue's model, the arc centre angle is larger and the radius is smaller, compared with the parameters of the real arc. As shown in Fig. 5, the red solid line represents the centre line and the arc of the deformed sealing disc predicted by O'Donoghue's model. The black dashed line represents the deformed sealing disc that is closer to the real condition. It can be observed that β is overestimated and R is underestimated. The deformation of the sealing disc around the separating disc is larger than that observed under ideal conditions. Therefore, a supplementary deflection angle was added in this study to improve the accuracy of the model.

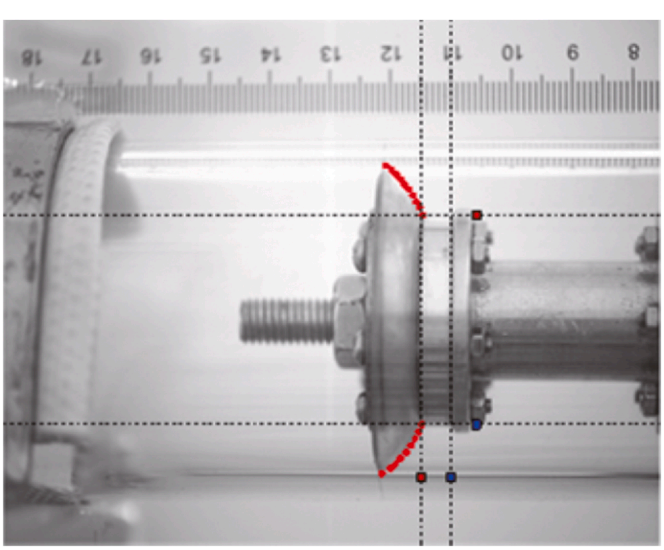

Fig. 4. Deformed sealing disc observed by a high-speed camera in the experiment.

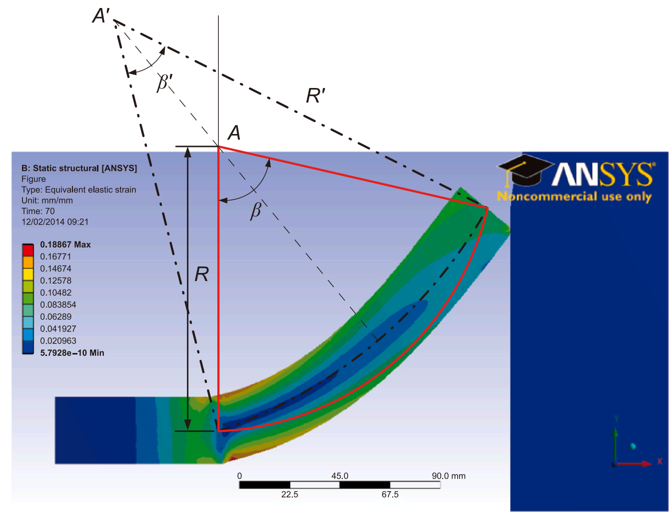

Fig. 5. Deformed sealing disc captured from the simulation result.

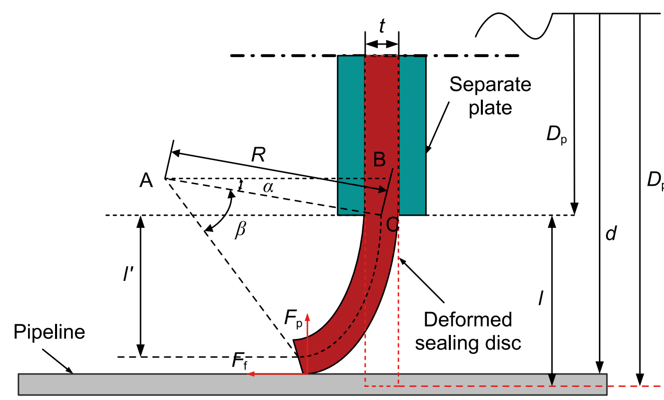

Fig. 6. Improved model for describing the deformation of the sealing disc.

2.2. Improved O'Donoghue model

As shown in Fig. 6, the sealing disc is deformed in an arc shape when pigging in the pipeline. β is the centre angle of the arc formed by the deformed sealing disc and was adopted in the O'Donoghue model. However, β' in Fig. 5 is the real centre angle, which is smaller than β, leading to a deviation. As a result, the auxiliary deflection angle α is added to the O'Donoghue's model, and the centre of the defected length of the sealing disc is reassessed, as shown in Fig. 6.

The model analyzed in this study was simplified into a 2D axisymmetric model. The separating disc was considered to be rigid in both the model and the experiment. Eq. (7) and Eq. (8) can be obtained from Fig. 6.

$$l = \frac{D_S - D_P}{2} \tag{7}$$

$$l' = \frac{d - D_P}{2} - \frac{t}{2}\sin(\alpha + \beta) \tag{8}$$

where α is the auxiliary angle of the arc ($\angle$BAC in Fig. 6) and AB is a line parallel to the axis of the pipeline.

As a result, Eq. (4) and Eq. (5) can be written as Eq. (9) and Eq. (10), respectively:

$$R \cdot \beta = l \tag{9}$$

$$R \cdot \sin(\alpha + \beta) - R \cdot \sin \alpha = l' \tag{10}$$

According to Eq. (9) and Eq. (10), as well as Eq. (7) and Eq. (8), the radius R formed by the deformed sealing disc can be expressed as Eq. (11):

$$R = \frac{l}{\beta} = \frac{l'}{\sin(\alpha + \beta) - \sin \alpha} = \frac{D_S - D_P}{2\beta} = \frac{d - D_P - t\sin(\alpha + \beta)}{2[\sin(\alpha + \beta) - \sin \alpha]} \tag{11}$$

where α and β are unknown, and $0 < \alpha < \pi/2$,$0 < \beta \le \pi$.

To propose a general mathematical model for evaluating α and β of the deformed sealing discs of different sizes, experiments and simulations are conducted in the following section.

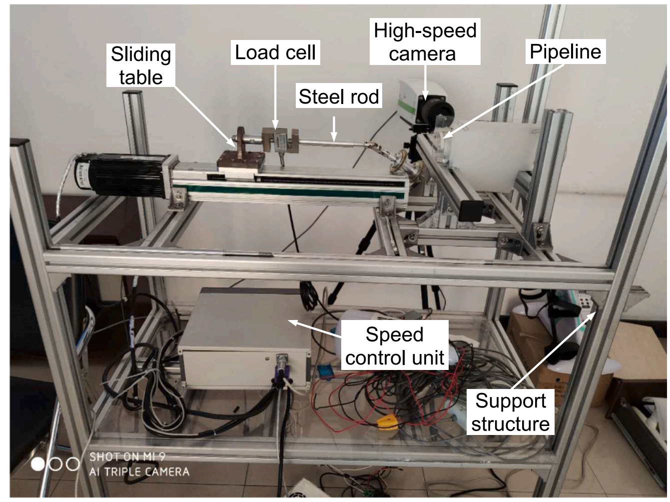

Fig. 8. Pig dragging experimental rig.

3. Experiment and simulation for measuring α and β

A pig dragging experiment was conducted at a constant speed to model stable pigging in the pipeline. A schematic of the rig is shown in Fig. 7, and the rig is shown in Fig. 8. Since the geometrical deformation of the sealing discs was investigated, which has nothing to do with the roughness and the friction coefficient. Plastic pipeline is used instead of the steel pipeline, for the observation by high-speed camera. Different sizes of sealing discs were used in the experiment to observe their deformation and a typical figure captured by a high-speed camera is shown in Fig. 4; then, α and β can be measured and fitted according to post-processing. A modified mathematical model to describe the deformation of the sealing disc can be achieved after obtaining α and β.

A numerical simulation with a 2D axisymmetric model was conducted using ANSYS (as shown in Fig. 9), in which α and β could be obtained as well. Subsequently, the simulation results were compared with the experimental results. After verifying the accuracy of the simulation results, the sealing discs of different size ratios were simulated to verify the modified mathematical model. The experimental and simulation details can be found in previous publications (Zhu et al., 2015a, 2015b, 2017a), which are not described in detail here for brevity. The sealing discs are made of polyurethane (PU). In order to obtain the constitutive model of PU with high accuracy, uniaxial tensile, uniaxial compression, and plane tensile tests were conducted, and the Mooney-Rivlin five-parameter constitutive model for simulating the deformation of the sealing disc was built and verified based on the test data, as shown in Fig. 10. A grid independence analysis was conducted as shown in Table 1. A quadrilateral mesh of 0.3 mm diameter was selected in the simulation.

Sealing discs with different interferences (δ), thickness per pipeline inner diameter (ξ) and clamping ratio (ζ) were investigated (shown in Table 2), where δ, ζ and ξ are all non-dimensional parameters and were expressed in Eqs. (12)–(14).

$$\delta = \frac{D_s - d}{d} \times 100\% \tag{12}$$

$$\zeta = \frac{D_p}{d} \times 100\% \tag{13}$$

$$\xi = \frac{t}{d} \times 100\% \tag{14}$$

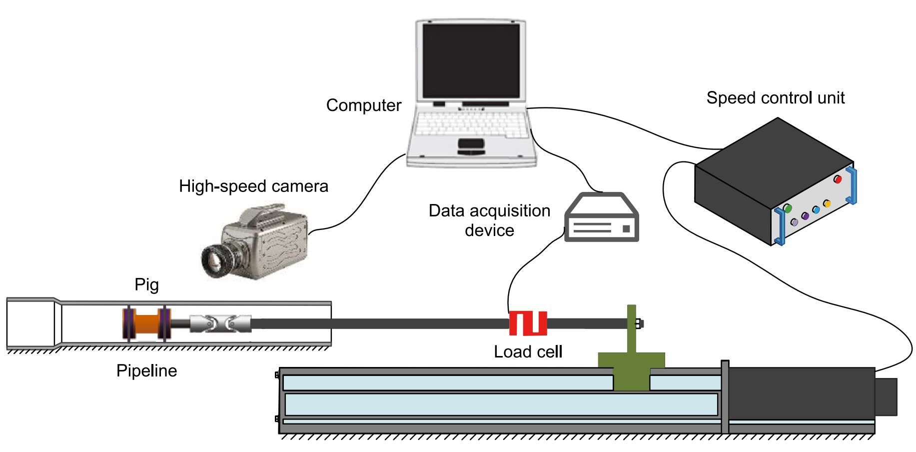

Fig. 7. Schematic diagram of the rig for pig dragging experiment.

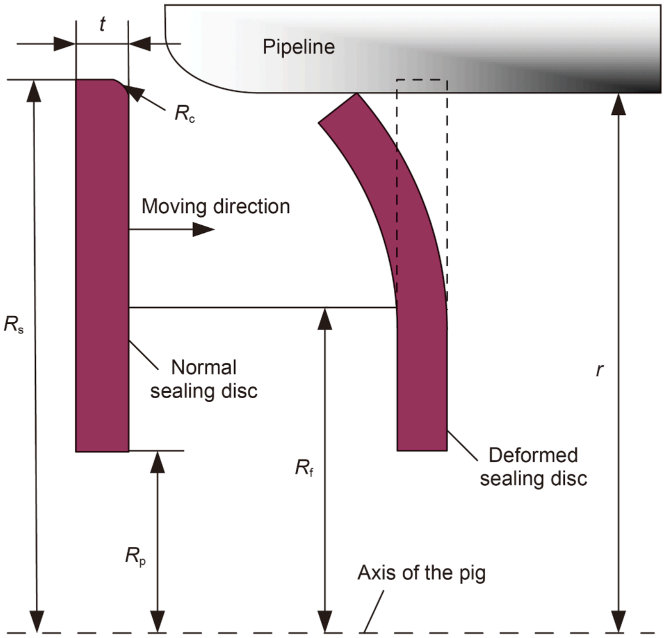

Fig. 9. Simplified 2D axisymmetric model used in the simulation (Zhu et al., 2015a).

3.1. Sealing discs with different interferences

When investigating the variation in α and β at different interferences ranging from 2% to 12% (the interference normally used in industry is 3%–5%), the outer diameter of the separating disc was 37 mm, and its thickness was 2 mm.

The profile of the deformed sealing disc was extracted from the experimental and simulation results by using GetData Graph Digitizer module in Origin software (as shown in Fig. 11), and the arc generated by the deflected length of the sealing disc was fitted using the least squares method in MATLAB. The centre position of the arc, α and β, can be obtained as well. The sealing disc is divided into the upper and lower halves in the experiment, as there are small changes in α and β in them owing to the effect of pig gravity.

As shown in Fig. 12, the results of α and β from the simulation agreed well with that from the experiment. With an increase in interference, a nearly linear increase in β can be observed. However, the variation in the interference had almost no effect on α.

3.2. The sealing discs with different thicknesses per inner diameter

Sealing discs with different thicknesses per inner diameter of the pipeline from 2% to 12% were investigated to observe the variations in α and β, as shown in Fig. 13. The outer diameters of the sealing disc and separating disc were 52 mm and 37 mm, respectively. Limited by the machining precision, the dimensional accuracy of the sealing disc with a thickness of 1 mm cannot be guaranteed. As a result, its experimental data with the thickness of 1 mm was dismissed.

Good agreement between α and β can be found in the simulation with the experiment, as shown in Fig. 14. In contrast to the effect of the interference, a small increment in α can be observed when the thickness per pipeline inner diameter increases from 2% to 10%. The sealing disc becomes harder to deform at larger thicknesses as the stiffness increases with an increment in the thickness (Zhu et al., 2015b). As a result, the arc becomes smaller,

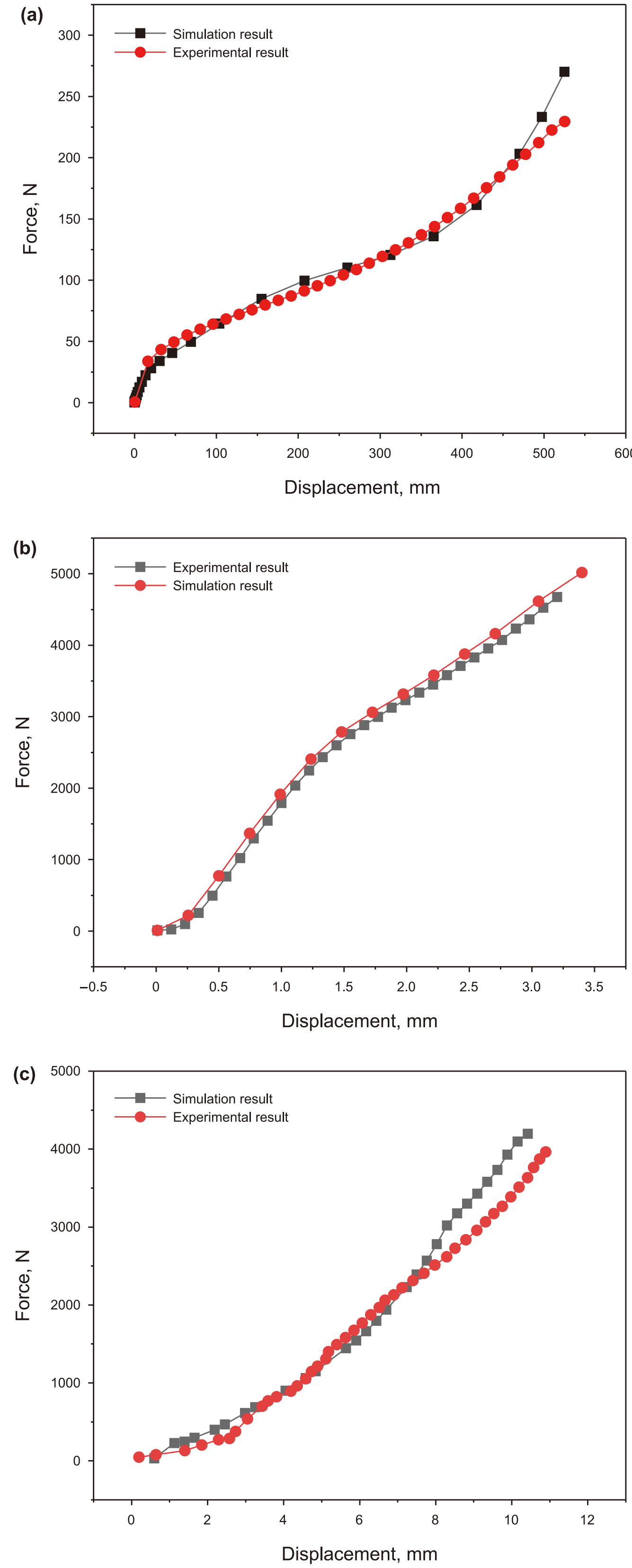

Fig. 10. Comparisons of the test data and simulation data: **(a)** tensile; **(b)** compression; **(c)** plane tensile.

Table 1
Grid independence analysis.

Grid size, mm	Number of grids	Grid quality	Simulated frictional force, N	Relative error, %
1.2	268	0.90934	57.160	0.335
1	285	0.92990	57.352	0.831
0.8	371	0.94498	57.829	0.401
0.4	922	0.96736	58.061	0.301
0.3	1242	0.97749	58.236	0.248
0.15	4344	0.99385	58.381	0.335

Table 2
Parameters of the sealing discs used in the experiment and simulation.

Parameter	Outer diameter of the sealing discs (D_s)	Thickness of the sealing discs (t)	Outer diameter of separating discs (D_p)
Value range, mm	51–57	1–5	35–45
Inner diameter of the pipeline (d, mm)	50		
Interference (δ)	2%–14%		
Thickness per pipeline inner diameter (ξ)		2%–10%	
Clamping ratio (ζ)			70%–90%

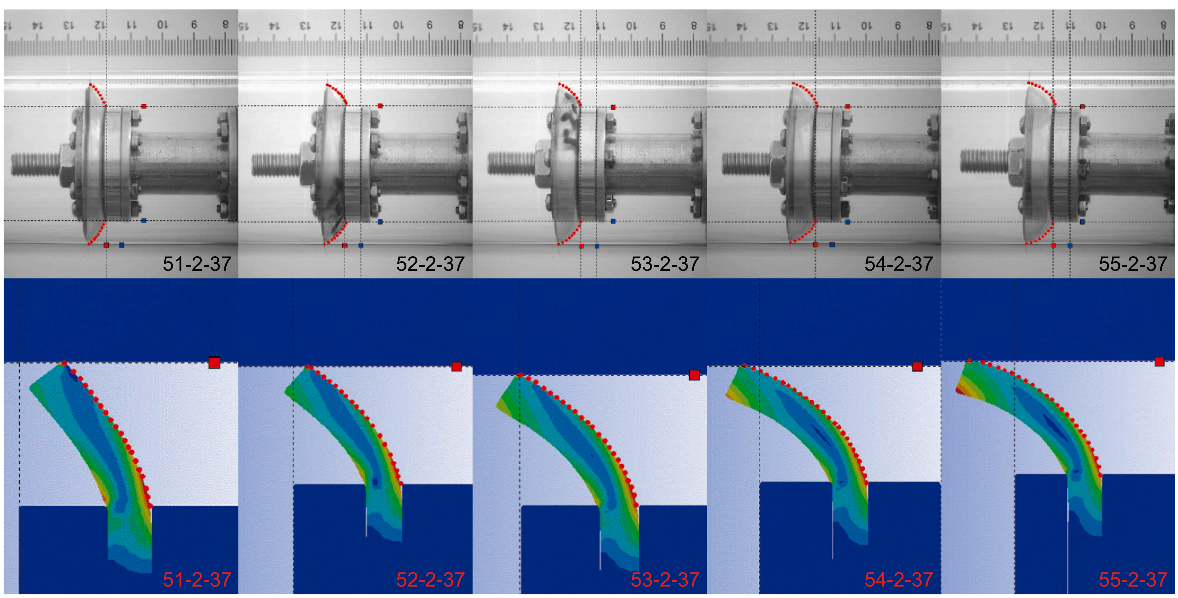

Fig. 11. The arc generated by the deflected length of the sealing disc from the experiment and simulation with different interference. Numbers at the corner of each figure mean D_s-t-D_p in Table 2.

and the radius increases, leading to a larger α to be compensated in the mathematical model.

3.3. The sealing discs with different clamping ratios

When the diameter and thickness of the sealing disc were 52 mm and 2 mm, respectively, the separating discs with outer diameters of 35–45 mm were introduced to investigate α and β at different clamping ratios, as shown in Fig. 15.

A comparison between α and β between the experimental and simulation data at different clamping ratios is shown in Fig. 16. A quadratic relationship between β and the clamping ratio can be observed, and the clamping ratio has almost no effect on α.

According to the relationship investigated above, the mathematical model for predicting the centre angle β of the arc formed by the deflected sealing disc can be written as Eq. (15):

$$\beta = a + b\cdot\xi + c\cdot\zeta^2 + d\cdot\zeta + e\cdot\delta \quad (15)$$

where a, b, c, d and e are the unknown variables that can be solved according to the data from the simulation and experiment. The fitting figure is shown in Fig. 17.

The correlation coefficient R^2 is 0.9883, and the final equation predicting β can be written as in Eq. (16):

$$\beta = 220.9989 + 2.473\cdot\xi + 0.0504\cdot\zeta^2 - 6.4633\zeta + 3.2774\delta \quad (16)$$

The auxiliary angle α is in the range of 14°–20° according to the results of the simulation and experiment. Consequently, the variation range of sinα was 0.2419–0.342. Although sinα has a range, its deviation from the final result of the model can be ignored. The value of α can be estimated appropriately based on experience. According to the analysis above, when the interference ranged from 2% to 14%, the clamping ratio was in the range 70%–90%, and the thickness per pipeline inner diameter, 2%–10%. The interference had the smallest effect on α, while the thickness per pipeline inner diameter had the greatest effect. Consequently, the influence of the thickness per pipeline inner diameter should be primarily

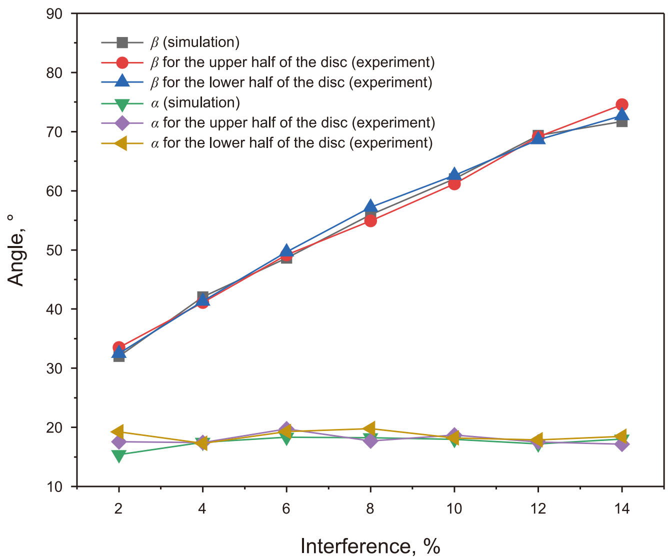

Fig. 12. Comparison of α and β between the experimental data and simulation data at different interferences.

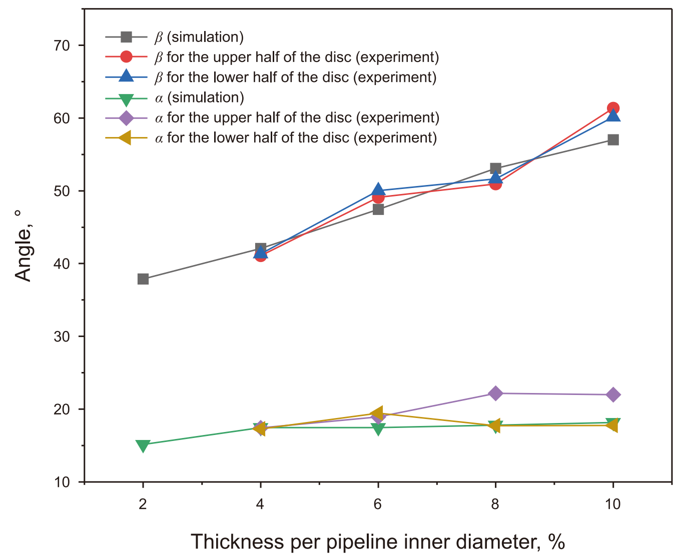

Fig. 14. Comparison of α and β between the experimental and simulation data at different thicknesses.

considered, followed by the influence of the clamping ratio, and finally, the influence of interference. A larger α can be selected for the sealing disc with a larger interference, thickness per pipeline inner diameter, or clamping ratio.

4. Mathematical model verification

In this section, two cases of different pigging sizes are introduced to verify the mathematical model. The first case is the sealing disc for 2-inch pipeline pigging, and the second case is the sealing disc for 40-inch pipeline pigging.

4.1. Case 1

Experiments were conducted on the sealing discs for 2inch pipeline pigging to obtain α and β at different interferences, thicknesses per pipeline inner diameter, and clamping ratios. The results were compared with those predicted from Eq. (16), as shown in Table 3.

Two groups of interference, thickness per pipeline inner diameter and clamping ratio, were used in the experiment, which were different from the groups used in Section 3. The comparison indicates that the mathematical model works well with a high

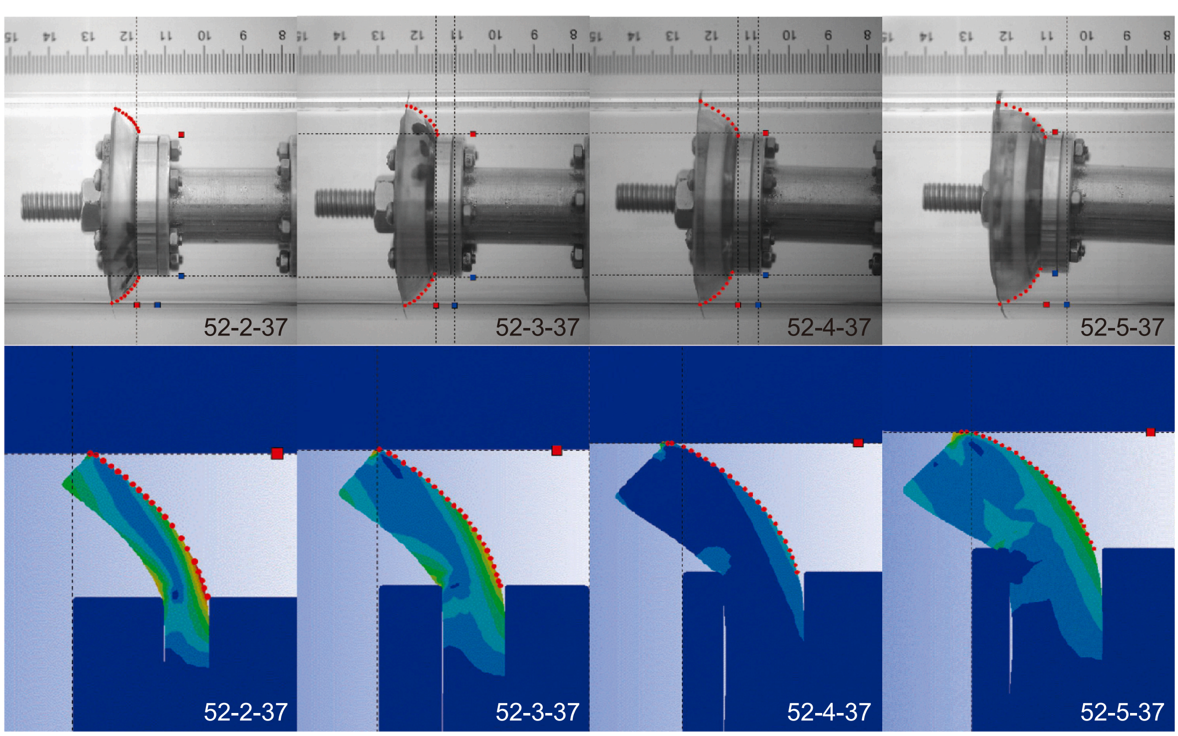

Fig. 13. The arc generated by the deflected length of the sealing disc from the experiment and simulation with different thicknesses per inner diameter.

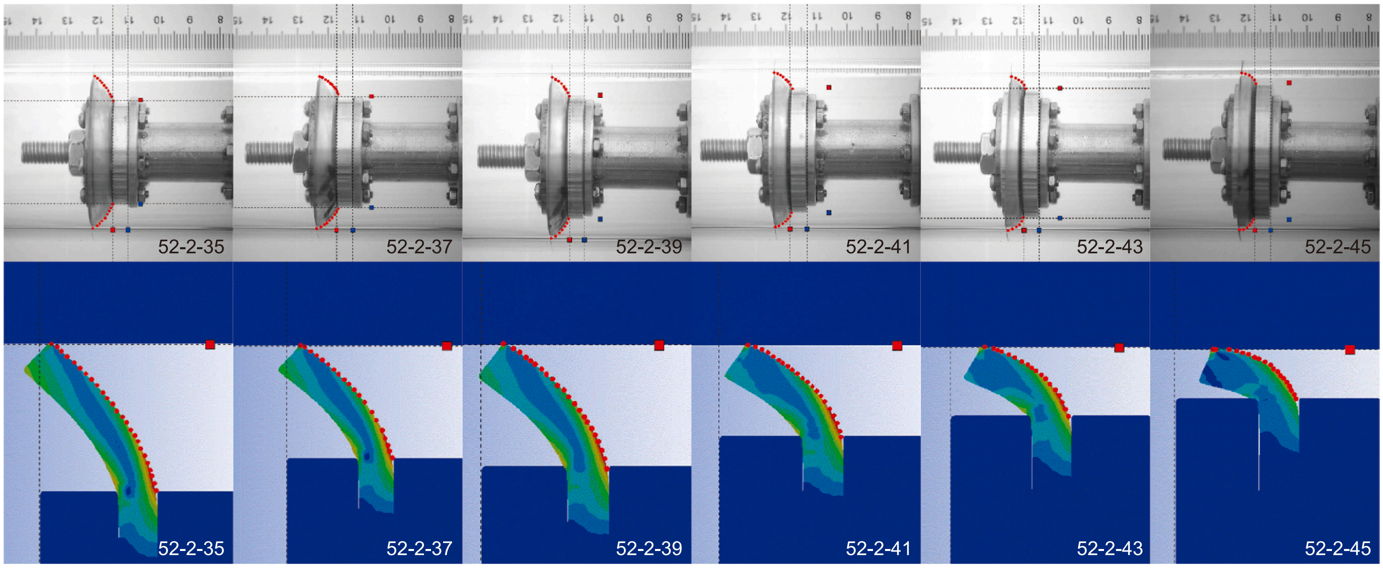

Fig. 15. The arc generated by the deflected length of the sealing disc from the experiment and simulation with different clamping ratios.

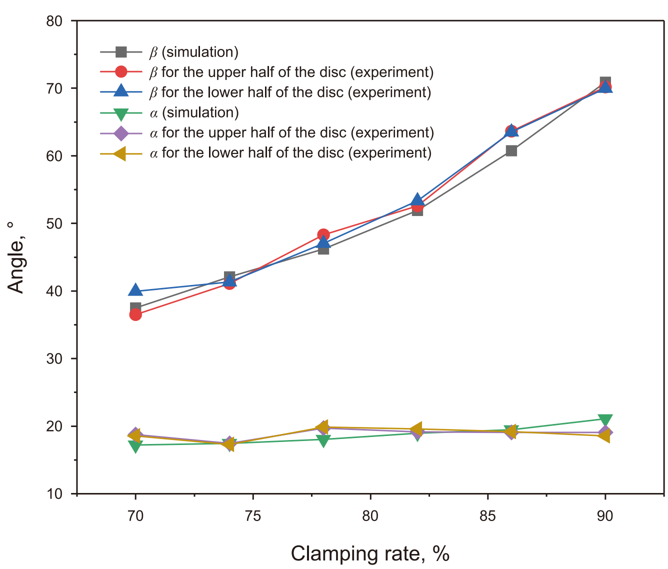

Fig. 16. Comparison of α and β between the experimental and simulation data at different clamping ratios.

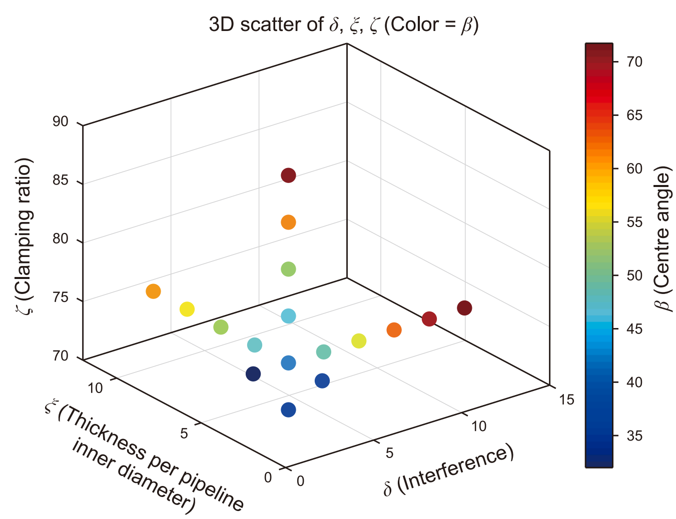

Fig. 17. Fitting variables of δ, ξ, and ζ

accuracy. Only 1.87% and 1.50% relative errors can be found with variations in these three parameters. 19.24° and 19.13° of α were observed in the simulation.

4.2. Case 2

In this case, the sealing discs for 40inch pipeline pigging are simulated to obtain α and β at different interferences, thicknesses per pipeline inner diameter, and clamping ratios, and then compared with the results predicted from the mathematical model. The comparisons are presented in Table 4.

Three groups of sealing discs of different sizes were investigated, and the maximum error of the mathematical model was observed to be 3.18%. An auxiliary angle α ranging from 14.44° to 16.51° can be observed within the range of 14°–20°. As mentioned in Section 3, a small auxiliary angle α can be selected when the clamping ratio is not large. Although there is approximately 6° deviation in the auxiliary angle α for the sealing discs with different sizes, the variation in sinα will be small and has little effect on Eqs. (7)–(11).

5. Conclusion

In this study, a modified model based on O'Donoghue's model is presented to describe the geometric deformation of a pig with sealing disc. The geometrical deformation of sealing disc under different sizes was observed and investigated when the interference is within 2%–14%, clamping ratio within 70%–90%, and thickness per pipeline inner diameter within 2%–10% (parameters used in the real condition were all contained). Owing to the limitation of the O'Donoghue's model for describing the geometrical deformation of the sealing disc under different sizes, an auxiliary angle α within 14°–20° is presented to improve the accuracy based on the experimental and simulation results. The improved mathematical model for predicting the centre angle β has been verified,

Table 3
Comparison of the results from the experiment and mathematical model for the sealing discs used in 2-inch pipeline pigging.

Outer diameter of sealing disc, mm	Outer diameter of separate plate, mm	Thickness of sealing disc, mm	Inner diameter of the pipeline, mm	β from experiment, °	β from mathematical model, °	Relative error, %	α from simulation, °
52	39	3	50	52.42	51.44	1.87	19.24
53	37	3		54.02	53.21	1.50	19.13

Table 4
Comparison of the results from simulation and mathematical model for the sealing discs used in 40-inch pipeline pigging.

Outer diameter of the sealing disc, mm	Outer diameter of the separating disc, mm	Thickness of the sealing disc, mm	Inner diameter of the pipeline, mm	β from simulation, °	β from mathematical model, °	Relative error, %	α from simulation, °
1020	600	25	986.8	32.54	31.63	2.80	14.44
1020	730	25		37.15	35.97	3.18	15.62
1030	730	30		41.83	40.55	3.06	16.51

and it can help build a mathematical model for predicting the frictional force of a bidirectional pig with higher accuracy.

CRediT authorship contribution statement

Xiao-Xiao Zhu: Writing – review & editing, Validation, Supervision, Software, Resources, Project administration, Methodology, Investigation, Funding acquisition, Formal analysis, Conceptualization. **Hao-Kun Wang:** Software, Formal analysis, Data curation. **Yi-Chen Zhang:** Writing – original draft, Software, Formal analysis, Data curation. **Chun-Ming Fu:** Writing – original draft, Software, Data curation. **Li-Yun Lao:** Writing – review & editing, Validation, Supervision, Methodology, Conceptualization.

Declaration of competing interest

The authors declare that they have no known competing financial interests or personal relationships that could have appeared to influence the work reported in this paper.

Acknowledgements

This work was supported by Key Technologies Research and Development Program (Grant No. SQ2022YFC2806103) and the National Natural Science Foundation of China (Grant No. 51509259).

References

Bai, C.Y., Zhang, J.J., 2013. Thermal, macroscopic, and microscopic characteristics of wax deposits in field pipelines. Energy Fuels 27 (2), 752–759. https://doi.org/10.1021/ef3017877.
Banki, R., Hoteit, H., Firoozabadi, A., 2008. Mathematical formulation and numerical modeling of wax deposition in pipelines from enthalpy-porosity approach and irreversible thermodynamics. Int. J. Heat Mass Tran. 51 (13–14), 3387–3398. https://doi.org/10.1016/j.ijheatmasstransfer.2007.11.012.
Botros, K.K., Golshan, H., 2009. Dynamics of pig motion in gas pipelines. In: AGA-Operations Conference & Biennial Exhibition, David L. Lawrence Convention Center. Pittsburgh Pennsylvania 1–16. May 19–21, 2009, Session 11: Corrosion Control.
Cao, Y.G., Zhen, Y., Shi, Y.J., Zhang, S.H., Sun, Y.T., Nie, W.J., 2018. Stress distribution of the power section cup of pipeline inspection gauges by finite element method. J. Pipeline Syst. Eng. Pract. 9 (2), 04017039. https://doi.org/10.1061/(asce)ps.1949-1204.0000308.
Chang, L., Cao, Y.G., Chen, J.Z., Dai, C.L., He, R.Y., Zhou, Z.G., 2023. The blockage risk in the elbow of the Bi-directional pig used for submarine pipeline based on the modified Burgers-Frenkel (MB-F) model. Ocean Eng. 268, 113508. https://doi.org/10.1016/j.oceaneng.2022.113508.
Ciszewski, M., Giergiel, M., Buratowski, T., Małka, P., 2020. Robotic inspection of pipelines. In: Ciszewski, M., Giergiel, M., Buratowski, T., Małka, P. (Eds.), Modeling and Control of a Tracked Mobile Robot for Pipeline Inspection. Springer International Publishing, Cham, pp. 5–21. https://doi.org/10.1007/978-3-030-42715-3_2.
Dai, B., Tao, Z., 2008. Research on abrasion and length characteristics of leather cap type pig. Transmission 2, 1–9.
de Souza, L.H.I., Silva, B.F., de Andrade, B.L.B., 2013. Analysis of contact forces acting upon pipelines pigs. In: COBEM 2013: 22nd International Congress of Mechanical Engineering Ribeirão Preto SP Brazil. PP. 9976–9784.
Den Heijer, A., 2016. Frictional Behaviour of Pigs in Motion. Master Thesis, Delft University of Technology.
Esmaeilzadeh, F., Mowla, D., Asemani, M., 2006. Modeling of pig operations in natural gas and liquid pipeline. In: SPE Annual Technical Conference and Exhibition. Society of Petroleum Engineers, San Antonio, Texas, USA, pp. 1–4. https://doi.org/10.2118/102049-ms.
Gao, X.D., Huang, Q.Y., Zhang, X., Zhang, Y., Zhu, X.R., Shan, J.X., 2021. Experimental study on the wax removal physics of foam pig in crude oil pipeline pigging. J. Petrol. Sci. Eng. 205, 108881. https://doi.org/10.1016/j.petrol.2021.108881.
Hendrix, M.H.W., Graafland, C.M., van Ostayen, R.A.J., 2018. Frictional forces for disc-type pigging of pipelines. J. Petrol. Sci. Eng. 171, 905–918. https://doi.org/10.1016/j.petrol.2018.07.076.
Lan, Z.C., Liu, S.H., Xiao, H.P., Wang, D.G., 2016. Frictional behavior of wax-oil gels. Tribol. Int. 96, 122–131. https://doi.org/10.1016/j.triboint.2015.12.027.
Lesani, M., Rafeeyan, M., Sohankar, A., 2012. Dynamic analysis of small pig through two and three-dimensional liquid pipeline. J. Appl. Fluid Mech. 5 (2), 75–83. https://doi.org/10.36884/jafm.5.02.12170.
Li, X.W., He, L.M., Luo, X.M., Liu, H.X., He, S.T., Li, Q.P., 2021. Transient pigging dynamics in gas pipelines: models, experiments, and simulations. Ocean Eng. 232, 109126. https://doi.org/10.1016/j.oceaneng.2021.109126.
Li, Q.P., Yao, H.Y., Chen, J.H., Luo, X.M., 2024. Bypass pigging technology in improving pigging safety and efficiency: principles, progress, and potentials. Int. J. Fluid Eng. 1 (2). https://doi.org/10.1063/5.0202414.
Liu, B., 2010. Research on Theory and Design of Gas-pipeline Inner Inspection PIG. PhD Thesis, China University of Petroleum.
Liu, H., Liu, Z., Taylor, B., Dong, H., 2019. Matching pipeline In-line inspection data for corrosion characterization. NDT E Int. 101, 44–52. https://doi.org/10.1016/j.ndteint.2018.10.004.
Liu, C., Cao, Y.G., Tian, H.J., Ma, S., 2021. A novel method for analyzing the driving force of the bi-directional pig based on the four-element model. Int. J. Pres. Ves. Pip. 190, 104314. https://doi.org/10.1016/j.ijpvp.2021.104314.
Liu, Y., Zhu, X.X., Song, J.P., Wu, H.Y., Zhang, S.F., Zhang, S.M., 2022. Research on bypass pigging in offshore riser system to mitigate severe slugging. Ocean Eng. 246, 110606. https://doi.org/10.1016/j.oceaneng.2022.110606.
Nguyen, T.T., Kim, D.K., Rho, Y.W., Kim, S.B., 2001a. Dynamic modeling and its analysis for PIG flow through curved section in natural gas pipeline. Proceedings 2001 IEEE International Symposium on Computational Intelligence in Robotics and Automation, pp. 492–497. https://doi.org/10.1109/cira.2001.1013250.
Nguyen, T.T., Kim, S.B., Yoo, H.R., Rho, Y.W., 2001b. Modeling and simulation for PIG flow control in natural gas pipeline. KSME Int. J. 15 (8), 1165–1173. https://doi.org/10.1007/bf03185096.
Nguyen, T.T., Kim, S.B., Yoo, H.R., Rho, Y.W., 2001c. Modeling and simulation for PIG with bypass flow control in nature gas pipeline. KSME Int. J. 15 (9), 1302–1310. https://doi.org/10.1007/bf03185671.
Niechele, A.O., Braga, A.M.B., Aevedo, L.F.A., 2000. Transient pig motion through non-isothermal gas and liquid pipelines. In: 2000 International Pipeline Conference. ASME, Calgary, Alberta, Canada, pp. 611–618. https://doi.org/10.1115/ipc2000-175.
Nieckele, A.O., Braga, A.M.B., Azevedo, L.F.A., 2001. Transient pig motion through gas and liquid pipelines. J. Energy Resour. Technol. 123 (4), 260–269. https://doi.org/10.1115/1.1413466.
O'Donoghue, A.F., 1996. On the Steady State Motion of Conventional Pipeline Pigs Using Incompressible Drive Media. PhD Thesis, Cranfield University.

Ohwoka, A.O., 2015. Polyurethane sealing discs on cleaning pigs-characterization and dynamic behaviour. Master Thesis.

Rahe, F., 2006. Optimizing the active speed control unit for in-line inspection tools in gas. In: Proceedings of the International Pipeline Conference, Calgary, IPC2006-10260. https://doi.org/10.1115/ipc2006-10260.

Romagnoli, R., Varvelli, R., 1991. Approach to the deformation study of pig cups. In: The First International Offshore and Polar Engineering Conference Edinburgh, United Kingdom, pp. 22–25.

Sadovnychiy, S., López, J., Ponomaryov, V., Sadovnychyy, A., 2006. Evaluation of distance measurement accuracy by odometer for pipelines pigs. J. Jpn. Petrol. Inst. 49 (1), 38–42. https://doi.org/10.1627/jpi.49.38.

Saeidbakhsh, M., Rafeeyan, M., Ziaei-Rad, S., 2009. Dynamic analysis of small pigs in space pipelines. Oil & Gas Science and Technology-Revue de l'IFP 64 (2), 155–164. https://doi.org/10.2516/ogst:2008046.

Solghar, A.A., Davoudian, M., 2013. Analysis of transient PIG motion in natural gas pipeline. Mechanics & Industry 13 (5), 293–300. https://doi.org/10.1051/meca/2012039.

Souza Mendes, P.R., Braga, A.M.B., Azevedo, L.F.A., Correa, K.S., 1999. Resistive force of wax deposits during pigging operations. J. Energy Resour. Technol. 121 (3), 167–171. https://doi.org/10.1115/1.2795977.

Tan, G.-B., Wang, D.-G., Liu, S.-H., Zhang, S.-W., 2014. Probing tribological properties of waxy oil in pipeline pigging with fluorescence technique. Tribol. Int. 71, 26–37. https://doi.org/10.1016/j.triboint.2013.10.020.

Tiratsoo, J., 1992. Pipeline Pigging Technology. Gulf Professional Publishing.

Tiratsoo, J., 2013. Pipeline pigging and integrity technology. Tiratsoo Technical.

Tolmasquim, S.T., Nieckele, A.O., 2008. Design and control of pig operations through pipelines. J. Petrol. Sci. Eng. 62 (3–4), 102–110. https://doi.org/10.1016/j.petrol.2008.07.002.

Wang, W.D., Huang, Q.Y., 2014. Prediction for wax deposition in oil pipelines validated by field pigging. J. Energy Inst. 87 (3), 196–207. https://doi.org/10.1016/j.joei.2014.03.013.

Wang, Q., Sarica, C., Chen, T.X., 2005. An experimental study on mechanics of wax removal in pipeline. J. Energy Resour. Technol. 127 (4), 302–309. https://doi.org/10.1115/1.2047591.

Wang, Q., Sarica, C., Volk, M., 2008. An experimental study on wax removal in pipes with oil flow. J. Energy Resour. Technol. 130 (4). https://doi.org/10.1115/1.3000136, 043001.

Wang, W.D., Huang, Q.Y., Pang, Q., Fu, J., Wang, F.H., 2014. Study of paraffin wax deposition in seasonally pigged pipelines. Chem. Technol. Fuels Oils 50 (1), 39–50. https://doi.org/10.1007/s10553-014-0488-2.

Wang, L., Bi, H., Yang, Y., Zhang, Y., Li, Y., 2018. Response analysis of an aerial-crossing gas-transmission pipeline during pigging operations. Int. J. Pres. Ves. Pip. 165, 286–294. https://doi.org/10.1016/j.ijpvp.2018.07.011.

Yu, T., Li, C.X., Yao, B., Zhang, Z.J., Guo, Y., Liu, L.J., 2020. Standard friction prediction model of long-distance hot oil pipelines. Pet. Sci. 17 (2), 487–498. https://doi.org/10.1007/s12182-019-00417-w.

Zhang, H., Gao, M.Q., Tang, B., Cui, C., Xu, X.F., 2022. Dynamic characteristics of the pipeline inspection gauge under girth weld excitation in submarine pipeline. Pet. Sci. 19 (2), 774–788. https://doi.org/10.1016/j.petsci.2021.09.044.

Zhao, H., Zhao, Y.X., Ye, Z.H., 2016. Interactions between the fluid and an isolation tool in a pipe: laboratory experiments and numerical simulation. Pet. Sci. 13 (4), 746–759. https://doi.org/10.1007/s12182-016-0123-4Actions.

Zhu, X.X., Wang, D.G., Yeung, H., Zhang, S.M., Liu, S.H., 2015a. Comparison of linear and nonlinear simulations of bidirectional pig contact forces in gas pipelines. J. Nat. Gas Sci. Eng. 27 (Part 1), 151–157. https://doi.org/10.1016/j.jngse.2015.08.048.

Zhu, X.X., Zhang, S.M., Li, X.L., Wang, D.G., Yu, D., 2015b. Numerical simulation of contact force on bi-directional pig in gas pipeline: at the early stage of pigging. J. Nat. Gas Sci. Eng. 23, 127–138. https://doi.org/10.1016/j.jngse.2015.01.034.

Zhu, X.X., Li, X.L., Zhao, C.H., Zhang, S.M., Liu, S.H., 2016. Dynamic simulation and experimental research on the motion of odometer passing over the weld. J. Nat. Gas Sci. Eng. 30, 205–212. https://doi.org/10.1016/j.jngse.2016.02.025.

Zhu, X.X., Wang, W., Zhang, S.M., Liu, S., 2017a. Experimental research on the frictional resistance of fluid-driven pipeline robot with small size in gas pipeline. Tribol. Lett. 65 (2), 49. https://doi.org/10.1007/s11249-017-0830-z.

Zhu, X., Wang, W., Zhang, S., Wang, C., 2017b. The pig gravity impact on its frictional force in oil and gas pipeline. In: The 27th International Ocean and Polar Engineering Conference. International Society of Offshore and Polar Engineers, San Francisco.

Zhu, X.X., Fu, C.M., Wang, Y.T., Zhang, S.M., 2023a. Experimental research on the contact force of the bi-directional pig in oil and gas pipeline. Pet. Sci. 20 (1), 474–481. https://doi.org/10.1016/j.petsci.2022.08.021.

Zhu, X.X., Fu, Y.L., Wang, Y.T., Wang, L.L., Lao, L.Y., 2023b. Research on the dynamic response of a steel catenary riser in the touchdown zone under pigging conditions. Energies 16 (15), 5832. https://doi.org/10.3390/en16155832.